Structural Change in Phosphorus-Bearing Dicalcium Silicates

Koichiro FUKUDA, Iwao MAKI, Suketoshi ITO and Takayuki MIYAKE†

Department of Materials Science and Engineering, Nagoya Institute of Technology, Gokiso-cho, Showa-ku, Nagoya-shi 466

リンを固溶したケイ酸カルシウムの構造変化

福田功一郎・牧　巖・伊藤祐敏・三宅孝行†

名古屋工業大学材料工学科，466 愛知県名古屋市昭和区御器所町

Structures of $(Ca_{2-x/2}\square_{x/2})(Si_{1-x}P_x)O_4$ crystals were examined as a function of x ranging from 0.03 to 0.40. All of the samples were heated at the stable temperature region of the α-phase and then quenched in water. The phase constitution at ambient temperature was classified into three categories according to the fraction of the α-to-α'_H transition. When the transition was completed as in the crystals with $x \leq 0.100$, the β- and α'_L-phases were obtained, the relative amounts of which were determined by the start and finish temperatures of the α'_L-to-β martensitic transformation. With $0.125 \leq x \leq 0.150$, the α-to-α'_H transition was incomplete. During further cooling, the product α'_H-phase was inverted to the α'_L-phase, and the residual α-phase was inverted to the incommensurate phase successively. Because the start temperature of the α'_L-to-β transformation was lower than ambient temperature, the α'_L-phase was stabilized. With $x \geq 0.175$, all of the crystals were free from the α-to-α'_H transition. The crystals with $0.175 \leq x \leq 0.225$ were made up exclusively of the incommensurate phase. A good correlation existed between the modulation wavelength $(=N)$ and the P/(Si+P) ratio $(=x)$ as $N=4.134-1.56x$ $(0.175 \leq x \leq 0.250)$. With $0.275 \leq x \leq 0.300$, the crystals were isostructural with α-Ca_2SiO_4. The hexagonal phase with $0.350 \leq x \leq 0.400$, probably a transition product from the α-phase, showed two-dimensional modulations along the a-axis with $N=2$ and along the c-axis with $N=3$.

[Received September 26, 1996; Accepted December 11, 1996]

Key-words : *Dicalcium silicates, Solid solutions, Crystal structures, Transformations, Modulations*

1. Introduction

The phase diagram in the binary system Ca_2SiO_4–$Ca_3(PO_4)_2$[1)-5)] shows that Ca_2SiO_4 (C_2S) incorporates certain amounts of phosphate to stabilize the high temperature modifications of β, α' and α with increasing phosphate content. When these Ca_2SiO_4 solid solutions (C_2S(ss)) were quenched from elevated temperatures, they, however, do not necessarily show exactly the same structures as the high temperature modifications. They sometimes show modulated distortions with incommensurate or commensurate superstructures.[4),6)-8)]

Incorporation of some kinds of foreign oxides into C_2S(ss) can effectively depress the transition rate of $\alpha \to \alpha'_H$ and the transformation temperatures of $\alpha'_L \to \beta$, leading to the stabilization of the high temperature modifications.[9)-12)] The transition of $\alpha \to \alpha'_H$ is an isothermal nucleation and growth process. The time and temperature for the start and finish of the transition have been represented by two C-shaped curves on the time–temperature–transformation (TTT) diagram.[10)] With increasing concentration of foreign oxides in solid solution, the time for the start of the transition and that for the finish increased steadily. By superimposing cooling curves on the TTT diagram, we can predict the intracrystalline microtexture as well as the constituent phases after cooling. The transformation of $\alpha'_L \to \beta$ is martensitic.[11)-13)] The reaction spontaneously begins at a definite temperature, M_s, and with decreasing temperature, the transformed fraction increases to M_f, at which the reaction is completed. Because the transformation is athermal, the fraction depended entirely on temperature; the phase constitution at ambient temperature (T_a) was determined to be α'_L ($M_s < T_a$), α'_L and β ($M_f \leq T_a \leq M_s$) and β ($T_a < M_f$).[12)] With increasing concentration of foreign oxides, the transformation temperatures of M_s and M_f decreased steadily.[11),12)]

An incommensurate orthorhombic phase has been obtained for the C_2S(ss) quenched from the stable temperature region of the α-phase.[4),6)-8),14)] In the reciprocal space, the reflections were expressed by

$$Q = h\boldsymbol{a}^* + k\boldsymbol{b}^* + l\boldsymbol{c}^* + n\boldsymbol{k} \qquad (1)$$

using four indices (h, k, l and n), and the wave vector $\boldsymbol{k}$ was redefined by $(1/N)\boldsymbol{a}^* + \boldsymbol{c}^*$ with N as the modulation wavelength.[8)] Commensurate modulations were reported for the hexagonal C_2S(ss) with P/(Si+P) = 0.398.[8)] They were $N=2$ along the a-axis and $N=3$ along the c-axis with reference to the underlying α-phase lattice.

The present study deals with the structural change with concentration of P_2O_5 in C_2S(ss) obtained by quenching from the stable temperature region of the α-phase.

2. Experimental

2.1 Materials

Fifteen kinds of mixtures were prepared from reagent-grade chemicals, $CaCO_3$, SiO_2 and $CaHPO_4 \cdot 2H_2O$. They were pressed into pellets, heated at 1500°C for 5 days and then quenched in water. The chemical formulae of the crystals obtained after heating were $(Ca_{2-x/2}\square_{x/2})(Si_{1-x}P_x)O_4$ with x ranging from 0.03 to 0.40 (Table 1). During heating, most of the crystal grains were developed larger than 50 μm (<400 μm) in diameter. The samples were termed S-A to S-O in the order of increasing x. Because these compositions varied along the line Ca_2SiO_4–$Ca_3(PO_4)_2$ on the binary phase diagram, they were also represented by $(1-y)$ $Ca_2SiO_4 \cdot y\,Ca_3(PO_4)_2$, where $y = x/(2-x)$ $(0.015 \leq y \leq 0.25)$.

2.2 Characterization

Thin sections were made of all the samples, and the intracrystalline microtextures were observed under an optical microscope.

Crystal grains of approximately 100 μm in diameter were selected for the Laue and precession method (samples S-J, S-K, S-M, S-N and S-O).

The powder X-ray diffraction (XRD) profiles were ob-

† Present address : Tsuruya Roofing Tile Co., Ltd., 2-12, Sunosaki-cho, Handa-shi, Aichi 475
現在：(株)鶴弥，475 愛知県半田市州の崎町 2-12

Table 1. Phase Constitution of the $(Ca_{2-x/2}\square_{x/2})(Si_{1-x}P_x)O_4$ Crystals

Category	I			II		III									
Sample	S-A	S-B	S-C	S-D	S-E	S-F	S-G	S-H	S-I	S-J	S-K	S-L	S-M	S-N	S-O
x	0.030	0.080	0.100	0.125	0.150	0.175	0.200	0.225	0.250	0.275	0.300	0.325	0.350	0.375	0.400
Phase	β	β	β + α'$_L$	α'$_L$+INC	α'$_L$+INC	INC	INC	INC	INC+α	α	α	α + H	H	H	H

INC: Incommensurate phase.
H: Hexagonal phase with modulations $N = 2$ along the a-axis and $N = 3$ along the c-axis.

tained on a diffractometer (Philips Co., Model PW3050) using monochromatized Cu Kα radiation (40 kV, 50 mA) and the step-scan technique (step width=0.02° and fixed time=10 s) in the 2θ range from 20 to 60°. Silicon powder was used as an internal standard (sample/Si=7 by weight). Peak positions were determined by fitting individual line profiles to the Pearson VII function on a computer program PRO-FIT.[15] With the crystals in S-A, S-B, S-J and S-K, the relative integrated intensities as well as the cell dimensions were refined by the whole-powder-pattern decomposition without reference to a structural model (WPPD) method.[15]

X-ray powder diffraction intensities of the incommensurate phase were found from calculation on a simulation mode of the computer program RIETAN.[16] The crystallographic DATA used were those determined by Saalfeld and Klaska,[6] who, assuming N=4, refined the structure of $6Ca_2SiO_4 \cdot 1Ca_3(PO_4)_2$ (x=0.250 and y=0.143) with N=3.75.

3. Results and discussion

3.1 Phase constitution with P/(Si+P) ratio

The phase constitution at ambient temperature (20°C) was classified into three categories (I, II and III) according to the fraction of the α-to-α'_H transition (Table 1). In accordance with the previous results,[10] the time for the start of the α-to-α'_H transition and that for the finish should increase steadily with increasing x. This leads to a systematic change in the transformed fraction when the crystals with various x-values were cooled at the same rate; the resulting phase constitution will be α'_H, $\alpha'_H+\alpha$ and α with increasing x. These phases may be inverted to thermodynamically more favorable phases during further cooling.

Powder XRD and thin-section observation showed that the crystals in S–A and S–B ($x\leq0.080$) were composed exclusively of the β-phase and those in S–C (x=0.100) of both the α'_L- and β-phases (Table 1). The intracrystalline lamella structure[17),18] within these crystals indicated that they were formed in the stable temperature region of the α-phase. Upon quenching, the phase transition of $\alpha \rightarrow \alpha'_H$ terminated and, during further cooling, the transitions of $\alpha'_H\rightarrow\alpha'_L\rightarrow\beta$ occurred successively. The martensitic transformation of $\alpha'_L\rightarrow\beta$ was completed within the crystals in S–A and S–B; however, it was incomplete within the crystals in S–C because the M_f was below ambient temperature. Accordingly, the M_f decreased with increasing x as 20°C$<M_f$ for $x\leq0.080$ and $M_f<$20°C for x=0.100.

The thin-section observation and precession photographs showed that the crystals in S–D and S–E ($0.125\leq x\leq0.150$) consisted of the α'_L-phase lamellae with the host incommensurate phase (Table 1). Both phases were twinned cyclically by 120° around the c-axis of the former α-phase.[8,14] This texture implied that the α-to-α'_H transition was incomplete; the parent α-phase underwent the transition to form the lamella structure, and the residual α-phase between the lamellae was subsequently inverted to the incommensurate phase. The α'_H-phase was further inverted to the α'_L-phase. Because the M_s was below ambient temperature, the α'_L-phase was stabilized. Thus, the compositional change of M_s was determined to be 20°C$<M_s$ for x=0.100 (sample S–C) and $M_s<$20°C for $x\geq0.125$.

All the crystals with $0.175\leq x\leq0.400$ were free from the transition of $\alpha\rightarrow\alpha'_H$ (Table 1). The crystals in S–F, S–G and S–H ($0.175\leq x\leq0.225$) were composed entirely of the incommensurate phase without the lamella structure, indicating that they were directly inverted from the α-phase. The crystals in S–J, S–K, S–L, S–M, S–N and S–O ($0.275\leq x\leq0.400$) were uniform without twinning under crossed polars. The powder XRD pattern of the crystal in S–I (x=0.250) was characterized by overlapping of those of the crystals in S–H (x=0.225) and S–J (x=0.275). Thus, the crystal must be composed of the two phases.

The compositional changes of M_s and M_f were as a result determined to be 20°C$<M_f$ for $x\leq0.080$, $M_f<$20°C$<M_s$ for x=0.100 and $M_s<$20°C for $x\geq0.125$. In martensitic transformations, deformation above M_s', which may be achieved by quenching large crystal grains rapidly as in the present samples, can result in the formation of the product phase.[19] Thus, the M_s temperatures as determined may be higher than those at which the crystals were pulverized. In the previous studies, the M_s temperatures of the powdered samples were determined by DTA[9),20] and high-temperature powder XRD.[12] A similar effect (i.e., grain-size effect) was observed for the tetragonal-to-monoclinic transition in ZrO_2 particles; the M_s was raised by increasing the particle size.[21),22]

3.2 Change in modulation wavelength of the incommensurate phase with P/(Si+P) ratio

The powder XRD intensities of the incommensurate phase found from calculation were in fair agreement with those observed. They are summarized in Table 2 together with the d-values.

The subcell dimensions of the crystals in S–F, S–G and S–H were determined from the reflections of 0220, 1120, 1300 and 2000 (Table 3). The diffraction profiles for 0220 and 1120 almost coincided with each other because the subcell was nearly orthohexagonal in geometry ($\sqrt{3}\,a_s/b_s\approx1$).

The superstructure reflection with indices $13\bar{1}1$ was relatively strong in intensity and overlapped no other reflections (Table 2). From Eq. (1), the reciprocal vector is given by

$$Q_{13\bar{1}1}=(1+1/N)a_s^*+3b_s^* \qquad (2)$$

The magnitude is determined from the peak position ($2\theta_{13\bar{1}1}$)

$$|Q_{13\bar{1}1}|=2\sin\theta_{13\bar{1}1}/\lambda \qquad (3)$$

where λ is the radiation wavelength. The $2\theta_{13\bar{1}1}$-values were 35.367° (S–F), 35.443° (S–G) and 35.467° (S–H). Substitution of Eq. (2) into Eq. (3) and separation of N given

$$N=[a_s\{(2\sin\theta_{13\bar{1}1}/\lambda)^2-(3/b_s)^2\}^{1/2}-1]^{-1} \qquad (4)$$

Table 2. Powder X-ray Diffraction Intensities Found from Calculation for the Incommensurate Phase: $(Ca_{1.875}\square_{0.125})(Si_{0.750}P_{0.250})O_4$ $(30° \leq 2\theta \leq 36°$, Cu $K\alpha_1)$

h	*k*	*l*	*n*	2θ (°)	d_{calc}(nm)	Int.
2	1	1	-1	30.36	0.2942	<1
1	1	3	-1	30.45	0.2933	4
1	0	2	0	30.92	0.2889	17
1	2	0	1	30.94	0.2888	1
1	3	1	-1	31.08	0.2875	13
1	2	-2	2	31.20	0.2865	<1
0	3	1	0	31.38	0.2848	5
0	3	0	1	31.66	0.2824	2
2	0	2	-1	31.70	0.2821	3
0	2	2	0	32.38	0.2763	37
1	1	2	0	32.39	0.2762	86
1	3	3	-2	32.48	0.2754	2
0	2	1	1	32.65	0.2741	<1
1	3	0	0	32.99	0.2713	100
2	0	0	0	33.03	0.2710	55
2	1	2	-1	33.13	0.2702	2
0	2	0	2	33.44	0.2677	2
1	3	2	-1	33.80	0.2650	1
1	2	-1	2	33.91	0.2642	<1
2	1	0	0	34.41	0.2604	<1
2	2	1	-1	34.66	0.2586	2
1	2	3	-1	34.73	0.2581	4
1	1	1	1	34.74	0.2580	2
1	3	-1	1	35.31	0.2540	8
1	3	1	0	35.58	0.2521	<1

Crystallographic data given by Saalfeld and Klaska.[6]
$a = 0.542$nm, $b = 0.940$nm, $c = 0.683$nm and $N = 4$.
The setting of axes differs from that given in the original article.

The modulation wavelengths determined by substitution in Eq. (4) of a_s, b_s and $\theta_{13\bar{1}1}$ are given in Table 3. A good correlation existed between N and x (Fig. 1). In the figure, the open square and open circles indicate the previous results.[6),8)] In the latter, the samples contained K_2O (0.12–0.25 mass%), Al_2O_3 (0.12–0.17 mass%) and Fe_2O_3 (0.63–0.69 mass%) in addition to P_2O_5. The incorporation of these oxides in solid solution may contribute to increasing the modulation wavelength, the increment of which is given by $\Delta N = 0.236 - 0.94x$.

3.3 Structures of the hexagonal phases

The intensity distribution on the Laue and upper-level

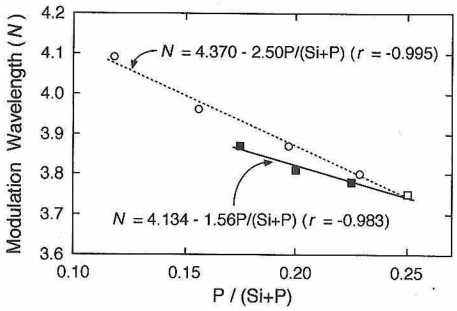

Fig. 1. Modulation wavelength (N) of the incommensurate phase as a function of P/(Si+P) ratio. (■) Present study (Samples S-F, S-G and S-H). (○,□) Previous studies.[6),8)] Crystals represented by the open circles were those doped with K_2O, Al_2O_3 and Fe_2O_3 in addition to P_2O_5.

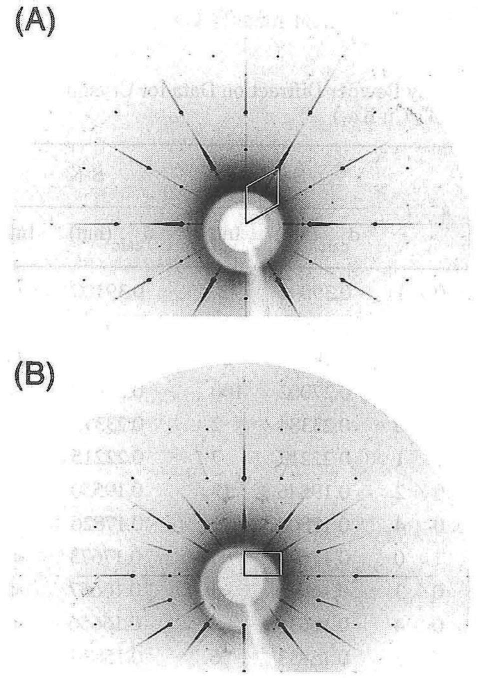

Fig. 2. Precession photographs of the single crystal in S-K. Incident beam parallel to c (A) and a (B). Heavy lines depict reciprocal unit-cells. Zero level, Zr-filtered Mo $K\alpha$, $\mu = 30°$.

Table 3. Crystallographic Data for C_2S(ss)

Sample	Crystal System	Modulation	Subcell Dimensions				
			a_s (nm)	b_s (nm)	c_s (nm)	β (°)	Volume (nm^3)
S-A	Monoclinic	None	0.55075(1)	0.67550(5)	0.93132(4)	94.273(4)	0.34552(5)
S-B	Monoclinic	None	0.55041(1)	0.67604(5)	0.93191(4)	93.994(4)	0.34592(5)
S-F	Orthorhombic	3.87*a*	0.5439(2)	0.9394(6)	0.6828(4)	---------	0.3489(3)
S-G	Orthorhombic	3.81*a*	0.5435(3)	0.9385(7)	0.6829(4)	---------	0.3483(4)
S-H	Orthorhombic	3.78*a*	0.5433(2)	0.9386(5)	0.6839(3)	---------	0.3487(3)
S-J	Hexagonal	None	0.54003(1)	---------	0.71216(3)	---------	0.17986(2)
S-K	Hexagonal	None	0.53991(1)	---------	0.71303(2)	---------	0.18000(1)
S-M	Hexagonal	2*a* and 3*c*	0.54071(3)	---------	0.7114(1)	---------	0.1801(1)
S-N	Hexagonal	2*a* and 3*c*	0.54030(7)	---------	0.7123(4)	---------	0.1801(1)
S-O	Hexagonal	2*a* and 3*c*	0.53992(3)	---------	0.7129(1)	---------	0.1800(1)

Figures in parentheses indicate standard deviations.

precession photographs of the crystals in S–J and S–K was consistent with hexagonal symmetry. The structure showed systematic absences $l \neq 2n$ for $hh\overline{2h}l$ and $l \neq 2n$ for $000l$ (Fig. 2). The probable space group is therefore $P6_3mc$, $P\bar{6}2c$ or $P6_3/mcc$. The cell dimensions (Table 3) and intensity distribution (Table 4) strongly suggest that these crystals are isostructural with α-C_2S.[23),24)]

The crystals in S–M, S–N and S–O were hexagonal and showed two-dimensional modulations along the a-axis with $N=2$ and along the c-axis with $N=3$. The subcell dimensions determined from the main reflections of 102, 110, 201, 202, 212 and 300 are given in Table 3. The superstructure showed systematic absences $l \neq 2n$ for $h\bar{h}0l$, $l \neq 2n$ for $hh\overline{2h}l$ and $l \neq 2n$ for $000l$; thus the probable space group is $P6cc$ or $P6/mcc$. These crystallographic data are in accord with those given by Fukuda et al.,[8)] who considered that their two-dimensionally modulated phase ($x=0.398$) was the transition product from the α-phase. The powder XRD patterns were very similar to that of the crystals composed of 66 mass% Ca_2SiO_4 and 34 mass% $Ca_3(PO_4)_2$ ($x=0.364$) by Nurse et al.[2)]

The subcell dimensions of the hexagonal phases (samples S–J to S–O) are plotted against x (Fig. 3). In the figure, the apparent subcell dimensions of the crystal in S–L ($a_s=0.54063(5)$ nm, $c_s=0.7120(3)$ nm and $V=0.1802(1)$ nm^3) are nearly intermediate between the dimensions of S–K (α-phase) and S–M (modulated hexagonal phase). Accordingly, the crystal must be the two-phase mixture. With the α- and modulated phases, the a-axis shrank and the c-axis expanded with increasing x. The volume increased for the α-phase, while it showed a tendency to decrease for the modulated phase with increasing x.

Table 4. X-ray Powder Diffraction Data for Crystals S–J and S–K ($20° \leq 2\theta \leq 60°$, Cu K$\alpha_1$)

h	k	l	S-J d_{calc}(nm)	S-J Int.	S-K d_{calc}(nm)	S-K Int.
1	0	1	0.39092	3	0.39100	4
0	0	2	0.35608	2	0.35651	2
1	0	2	0.28331	27	0.28350	29
1	1	0	0.27002	100	0.26995	100
2	0	0	0.23384	2	0.23379	1
2	0	1	0.22217	7	0.22215	8
2	0	2	0.19546	13	0.19550	14
0	0	4	0.17804	1	0.17826	2
2	1	0	0.17677	<1	0.17673	<1
2	0	3	0.16659	<1	0.16667	<1
1	0	4	0.16639	<1	0.16656	<1
2	1	2	0.15833	6	0.15834	6
3	0	0	0.15589	6	0.15586	7

The integrated intensities and unit-cell dimensions (Table 3) refined by the WPPD method. The reliability factors are R_p=0.0781, R_{wp}=0.1004 and R_p(peak)=0.1758 for S-J, and R_p=0.0777, R_{wp}=0.0990 and R_p(peak)=0.1797 for S-K.

4. Conclusions

(1) The phase constitution at ambient temperature, depending entirely on the P/(Si+P) ratio ($=x$), was classified into three categories according to the fraction of the α-to-α'_H transition.

(2) Both the start and finish temperatures of the α'_L-to-β martensitic transformation decreased with increasing x; $20°C < M_f$ for $x \leq 0.080$, $M_f < 20°C < M_s$ for $x=0.100$ and $M_s < 20°C$ for $x \geq 0.125$.

(3) The incommensurate phase showed a good correlation between modulation wavelength ($=N$) and x as $N=4.134-1.56x$ ($0.175 \leq x \leq 0.250$).

(4) With $0.275 \leq x \leq 0.300$, the quenched crystals were probably isostructural with the α-C_2S.

(5) The hexagonal phase with $0.350 \leq x \leq 0.400$ showed two-dimensional modulations ($N=2$ along the a-axis and $N=3$ along the c-axis), indicative of the transition product of the α-phase.

Acknowledgment This work was supported financially by the Cement Association of Japan.

References

1) R. E. Barrett and W. J. McCaughley, *Am. Mineral.*, 27, 680–95 (1942).
2) R. W. Nurse, J. H. Welch and W. Gutt, *J. Chem. Soc.*, 220, 1077–83 (1959).
3) W. Fix, H. Heymann and R. Heinke, *J. Am. Ceram. Soc.*, 52, 346–47 (1969).
4) H. Saalfeld, *Z. Kristallogr.*, 133, 396–404 (1971).
5) M. W. Barnes, M. Klimkiewicz and P. W. Brown, *J. Am. Ceram. Soc.*, 75, 1423–29 (1992).
6) H. Saalfeld and K. H. Klaska, *Z. Kristallogr.*, 155, 65–73 (1981).
7) K. Fukuda and I. Maki, *J. Am. Ceram. Soc.*, 72, 2204–07 (1989).
8) K. Fukuda, I. Maki, S. Ito, H. Yoshida and K. Aoki, *J. Am. Ceram. Soc.*, 77, 2615–19 (1994).
9) G. Lai, T. Nojiri and K. Nakano, *Cem. Concr. Res.*, 22, 743–54 (1992).

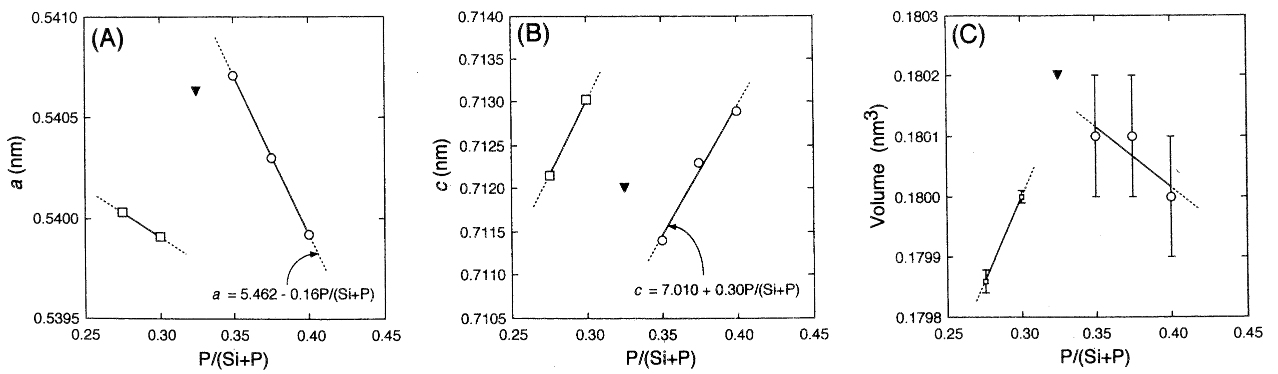

Fig. 3. Variation in subcell dimensions with P/(Si+P) ratio. a (A), c (B) and volume (C). (□) α-phase (Samples S–J and S–K). (○) Hexagonal phase with two-dimensional modulations (S–M, S–N and S–O). (▼) The two-phase mixture (S–L). Error bars indicate 1σ.

10) K. Fukuda, I. Maki, K. Toyoda and S. Ito, *J. Am. Ceram. Soc.*, 76, 1821–24 (1993).
11) K. Fukuda, I. Maki and S. Ito, *J. Am. Ceram. Soc.*, 79, 2925–28 (1996).
12) K. Fukuda, I. Maki and S. Ito, *J. Am. Ceram. Soc.*, 79, 2969–70 (1996).
13) Y. J. Kim, I. Nettleship and W. M. Kriven, *J. Am. Ceram. Soc.*, 75, 2407–19 (1992).
14) K. Fukuda, I. Maki and K. Adachi, *J. Am. Ceram. Soc.*, 75, 884–88 (1992).
15) H. Toraya, *J. Appl. Crystallogr.*, 19, 440–47 (1986).
16) F. Izumi, "The Rietveld Method," Oxford University Press (1993) pp. 236–53.
17) K. Fukuda and I. Maki, *Cem. Concr. Res.*, 19, 913–18 (1989).
18) K. Fukuda and I. Maki, *Cem. Concr. Res.*, 23, 599–602 (1993).
19) J. W. Christian, "The Theory of Transformations in Metals and Alloys," Pergamon Press (1975).
20) G. Yamaguchi, Y. Ono, S. Kawamura and Y Soda, *Yogyo-Kyokai-Shi*, 71, 21–26 (1963).
21) D. L. Porter and A. H. Heuer, *J. Am. Ceram. Soc.*, 62, 298–305 (1979).
22) A. H. Heuer, N. Claussen, W. M. Kriven and M. Rühle, *J. Am. Ceram. Soc.*, 65, 642–50 (1982).
23) G. Yamaguchi, Y. Ono, S. Kawamura and Y. Soda, *Yogyo-Kyokai-Shi*, 71, 105–08 (1963).
24) M. Regourd, M. Bigaré, J. Forest and A. Guinier, Proc. 5th Int. Symp. Chem. Cement, Tokyo, Cement Association of Japan (1968) pp. 44–48.